Numerical Modelling of MHD Space Plasmas

Hans De Sterck

Scalable Scientific Computing Group
Department of Applied Mathematics
University of Waterloo, Waterloo, Canada

DASP - CAP Congress 2010
Toronto, Ontario, Canada, June 6-11, 2010

Collaborators

University of Waterloo

- Lucian Ivan (postdoc)

University of Toronto

- Prof. Clinton Groth
- Scott Northrup
- CFD & Propulsion Group, Institute for Aerospace Studies

CSA Canadian Geospace Monitoring (CGSM) Program

Project: “Solar Drivers of Space Weather: Contributions to Forecasting”

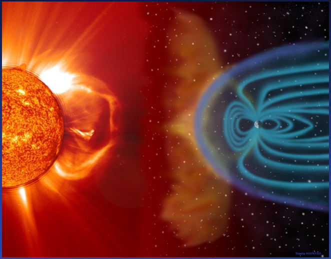

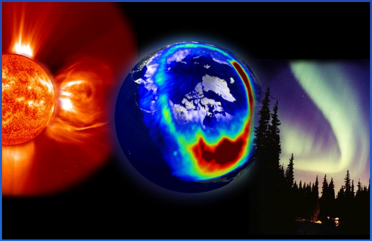

Images courtesy of SOHO/EIT consortium

Goal: Develop advanced simulation methods for MHD space plasmas and apply to space-weather forecasting

Housed At: Applied Math., U. Waterloo

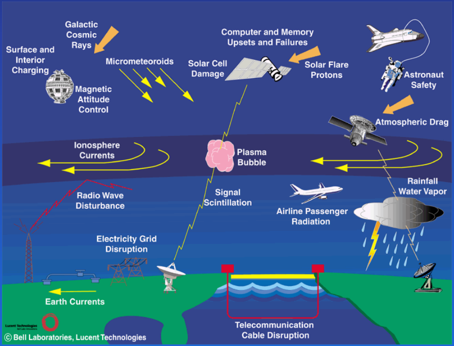

Image courtesy of NASA

MHD Equations

Ideal MHD Plasma

- magnetized, inviscid, fully ionized, compressible gas
- quasi-neutral, isotropic pressure, perfect gas (i.e. $p = \rho RT$)

Flow Governed by 3D Compressible MHD Equations

$$\frac{\partial \mathbf{U}}{\partial t} + \vec{\nabla} \cdot \vec{\mathbf{F}} = \mathbf{S}$$

Conserved solution state: $\mathbf{U} = \left[\ \rho,\ \ \rho\vec{u},\ \ \vec{B},\ \ \rho e\ \right]^{\mathrm{T}}$

Flux dyad: $\vec{\mathbf{F}} = \Big[\ \rho\vec{u},\ \ \rho\vec{u}\vec{u} + (p + \vec{B}\cdot\vec{B}/2)\vec{\vec{I}} - \vec{B}\vec{B},$
$\vec{u}\vec{B} - \vec{B}\vec{u},\ \ (\rho e + p + \vec{B}\cdot\vec{B}/2)\vec{u} - (\vec{u}\cdot\vec{B})\vec{B}\ \Big]^{\mathrm{T}}$

Spherically symmetric gravitational field: $\mathbf{S} = -\frac{\rho G M_*}{r^3}\left[\ 0,\ \ \vec{r},\ \ 0,\ \ \vec{r}\cdot\vec{u}\ \right]^{\mathrm{T}}$

CSA Canadian Geospace Monitoring (CGSM) Program

Project: "Solar Drivers of Space Weather: Contributions to Forecasting"

In Collaboration with:

- Prof. Groth's Group (CFFC Computational Framework)
- NRCan Geomagnetic Laboratory (Modeling & Validation)
- Others (e.g. Space Weather Forecasting 'in the cloud')

CSA Canadian Geospace Monitoring (CGSM) Program

Project: "Solar Drivers of Space Weather: Contributions to Forecasting"

Computational Framework Features/Design Goals

- **CFFC**: **C**omputational **F**ramework for **F**luids and **C**ombustion
- Hybrid unstructured-structured multi-block mesh
  our approach: **"cubed sphere"**
- Dynamic adaptive mesh refinement (**AMR**)
- Parallel and highly scalable implementation
- Implicit timestepping-multigrid/multilevel acceleration
- 2nd-, 3rd- and 4th-order accuracy
- Hardware accelerators: GPU computing

Discretizations of Spherical Domains

Several Options in the Literature

- Latitude-longitude grid constructs
- Cubed sphere
- Cartesian cut-cell approach
- Geodesic grid (e.g. icosahedron)

Discretizations of Spherical Domains

Latitude-Longitude Grid Constructs

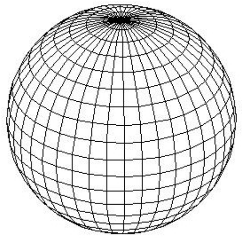

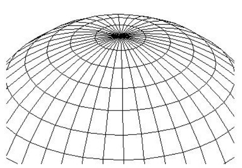

Advantages

- Natural basis for spherical flows
- Logically rectangular grid (r, θ, ϕ)
- Suitable for application of spectral methods
- Fairly uniform away from poles

Issues ("pole problems")

- Singularities at the poles, non-uniform
- Severe time-step restrictions
- Parallelization difficulties

Discretizations of Spherical Domains

Gnomonic Projection Based Grids

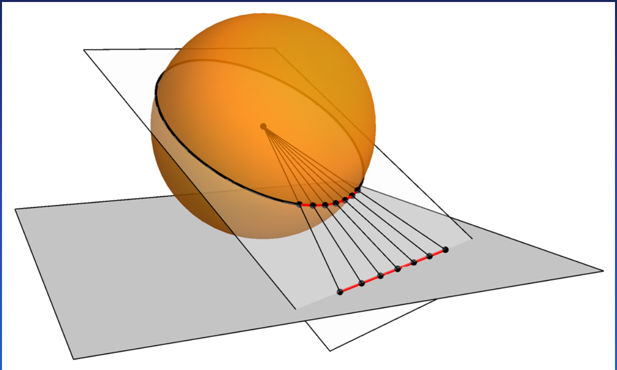

- Great circles are mapped into straight lines and vice-versa

Discretizations of Spherical Domains

"Cubed Sphere"

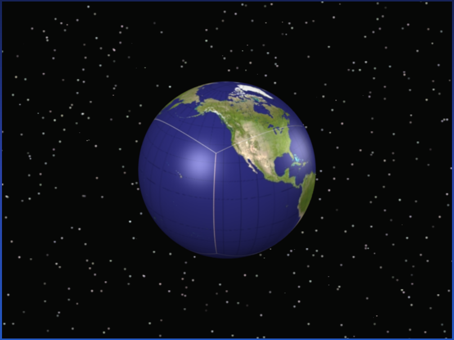

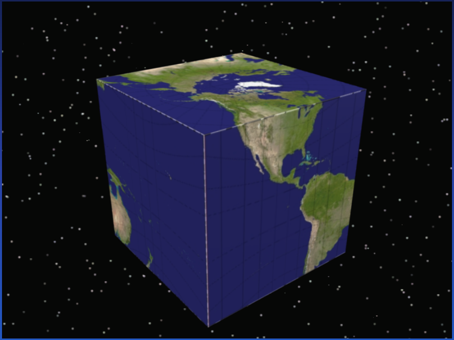

- The inverse projection maps the 6 straight faces of the cube into 6 adjoining spherical faces free of any strong singularities
- Natural application of a multi-block mesh data structure

Types of Cubed-Sphere Grids

Sadourny, 1972; Ronchi *et. al.*, 1996

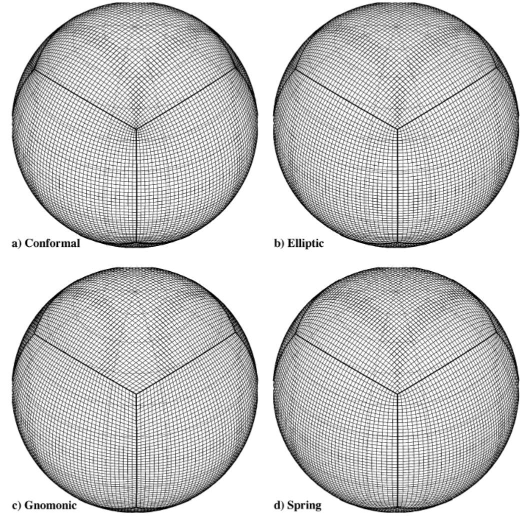

Image reproduced from Putman & Lin JCP2007

Gnomonic Grid

- The most uniform
- Equiangular or equidistant projection
- Min. length scales with increasing resolution
- Highly non-orthogonal and non-conformal
- Does not require extra meshing algorithms
- Accurate results with adequate schemes (Putman & Lin, 2007)
- Suitable for AMR

3D Cubed-Sphere Multi-Block Mesh in CFFC

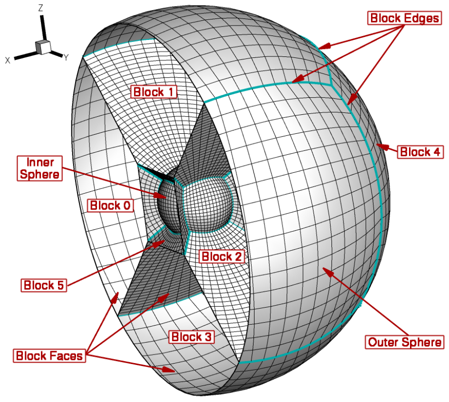

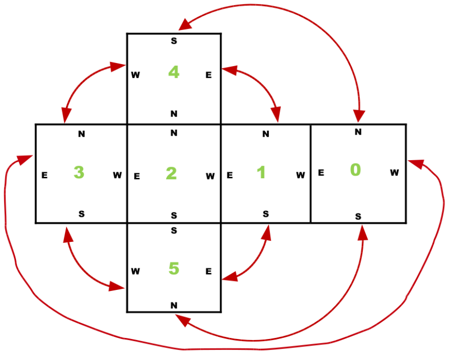

Cross-section of the cubed-sphere grid (**left)** and illustration of connectivity among blocks (**right)**

Finite-Volume Formulation

Semi-Discrete Integral Form for Hexahedral Cell (i,j,k)

$$\frac{d\mathbf{U}_{i,j,k}}{dt} = -\frac{1}{V_{i,j,k}} \sum_{m=1}^{N_f} \left(\int \vec{\mathbf{F}} \cdot \vec{n}\, dA \right)_{i,j,k,m} + (\mathbf{S})_{i,j,k}$$

Key Elements of Numerical Scheme

- High-order spatial discretization (2nd, 3rd, 4th)
- Multi-dimensional k-exact least-squares reconstruction (Barth, 1993) and limiters (Barth-Jespersen, 1993; Venkatakrishnan, 1993)
- Upwinding flux evaluation (Roe's 1981; HLLE 1983)
- Multi-stage explicit time marching schemes
- Parallel implicit NKS algorithms (Northrup & Groth 2009)

Finite-Volume Formulation

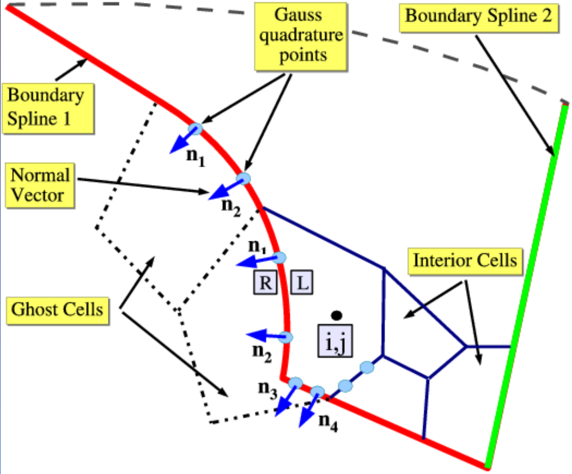

$$\frac{d\mathbf{U}_{i,j,k}}{dt} = -\frac{1}{V_{i,j,k}} \sum_{m=1}^{N_f} \left(\int \vec{\mathbf{F}} \cdot \vec{n}\, dA \right)_{i,j,k,m} + (\mathbf{S})_{i,j,k}$$

Finite-Volume Formulation

Overview of High-Order Benefits

What is Meant by High-Order?

- Schemes with order of truncation error greater than 2
- Spatial discretization error: $\mathcal{O}(\Delta x^n), n > 2$

High-Order Schemes vs. Low-Order Methods

- Less numerical dissipation & dispersion
- Require fewer mesh points to accurately resolve solution
- Potentially less expensive
- Trade-offs: Order of accuracy vs. computational cost
- Our target: 4th-order accurate solutions ($n = 4$)

Work in Concert with Other Strategies for Coping with High Computational Cost

- Adaptive Mesh Refinement (AMR)
- Efficient parallel solution schemes

Finite-Volume Formulation

k-exact Reconstruction (Barth, 1993)

- Piecewise polynomial approximation

$$u_{i,j}^{k}(\vec{r}) = \sum_{p_1=0}^{N_1} \sum_{p_2=0}^{N_2} (x - \bar{x}_{i,j})^{p_1} \, (y - \bar{y}_{i,j})^{p_2} \, D_{p_1 p_2}^{k} \quad , \quad N1 + N2 \leq k$$

- Satisfies the following conditions:
  - reconstruct exactly polynomials of degree $\leq k$

$$u_{i,j}^{k}(\vec{r} - \vec{\bar{r}}_{i,j}) - u(\vec{r}) = \mathcal{O}(\Delta x^{k+1})$$

  - conserve the mean solution

$$\iint\limits_{\mathcal{A}_{i,j}} u_{i,j}^{k}(\vec{r} - \vec{\bar{r}}_{i,j}) \, dxdy = \iint\limits_{\mathcal{A}_{i,j}} u(\vec{r}) \, dxdy$$

  - have compact support

Finite-Volume Formulation

Computation of Reconstruction Coefficients, $D^k_{p_1p_2}$

- Error, $Err_{\gamma,\delta}$, in each control volume, $CV_{\gamma,\delta}$, is minimized using least-squares formulation:

$$Err_{\gamma,\delta} = \frac{1}{A_{\gamma,\delta}} \iint\limits_{\mathcal{A}_{\gamma,\delta}} u^k_{i,j}(\vec{r} - \vec{\bar{r}}_{i,j})\, dxdy - \bar{u}_{\gamma,\delta}$$

- Results in linear equality-constrained least squares problem:

$$\mathbf{Ax} - \mathbf{b} = \mathbf{r}$$

- Solution of overdetermined linear system of equations:
  - Gaussian elimination + Householder QR factorization (or: compute the pseudo-inverse $\mathbf{A}^{-1}$)
- remove oscillations at discontinuities: detect discontinuities and reduce order (limited piecewise linear) (CENO scheme)

Finite-Volume Formulation

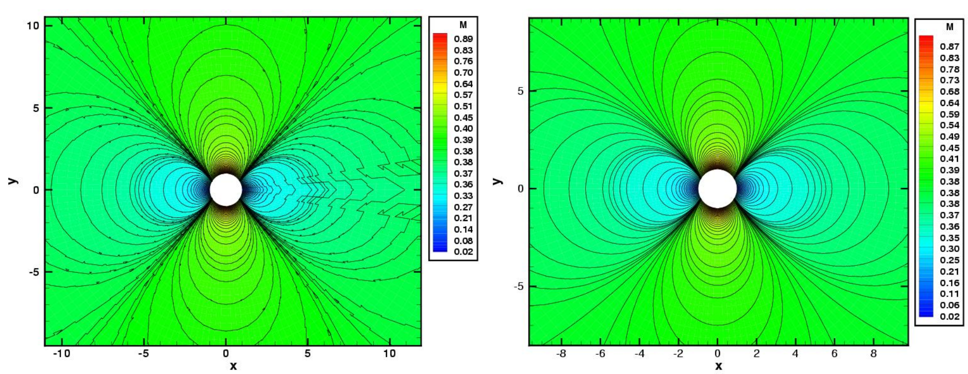

The Mach number prediction for the inviscid flow past a cylinder at $M = 0.38$ obtained with the 2nd- and 4th-order CENO on a mesh with 80x40 cells

Finite-Volume Formulation

2nd vs. 4th Order Accuracy: 2D Example to Illustrate Potential Benefits

Exact solution

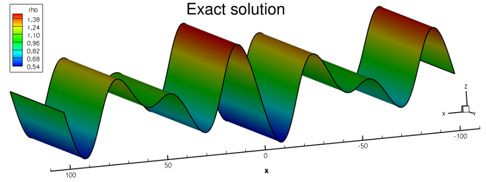

4th-order CENO solution after one period

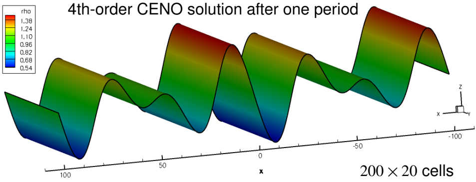

200×20 cells

# Cells	$\mathcal{O}(\Delta x^2)$		$\mathcal{O}(\Delta x^4)$	
4,000 (200x20)	$L1$:	2.68E-02	$L1$:	1.85E-04
	$L2$:	3.26E-02	$L2$:	2.18E-04
	$LMax$:	7.36E-02	$LMax$:	9.46E-04
	$Time$:	0:01:20	$Time$:	**0:10:38**
	Mem:	20,336	Mem:	**31,232**
8,000 (400x20)	$L1$:	9.38E-03	$L1$:	1.32E-05
	$L2$:	1.16E-02	$L2$:	2.02E-05
	$LMax$:	2.98E-02	$LMax$:	2.11E-04
	$Time$:	0:04:18	$Time$:	0:41:03
	Mem:	30,000	Mem:	50,816
80,000 (4000x20)	$L1$:	1.10E-04	$L1$:	-
	$L2$:	2.20E-04	$L2$:	-
	$LMax$:	1.33E-03	$LMax$:	-
	$Time$:	**8:23:38**	$Time$:	-
	Mem:	**203,680**	Mem:	-

Parallel Adaptive Finite-Volume Framework

Block-Based AMR Using Hierarchical Data Structure (Berger 1984; Gao & Groth 2010)

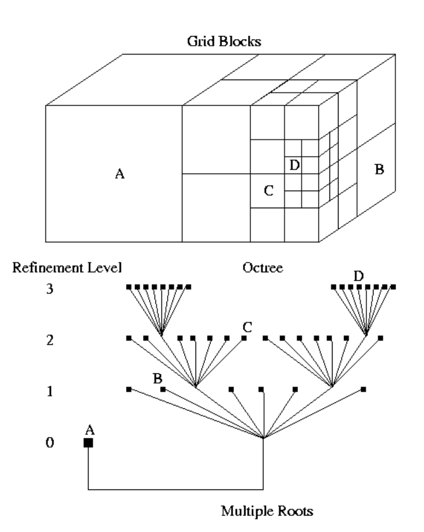

- Mesh refinement by division and coarsening of self-similar structured blocks (hexahedral cells)
- Hierarchical octree data structure provides block connectivity
- Solution transfer among blocks via overlapping ghost cells
- Permits local refinement of mesh
- Physics-based refinement criteria (e.g. $\epsilon_1 \propto |\vec{\nabla}\rho|$, $\epsilon_2 \propto |\vec{\nabla}\cdot\vec{u}|$, $\epsilon_3 \propto |\vec{\nabla}\otimes\vec{u}|$)
- Permits parallel implementation via domain partitioning
- Highly efficient load balancing is obtained by equally distributing the solution blocks among CPUs

Parallel Adaptive Finite-Volume Framework

AMR of Cubed-Sphere Grid

Previous Work

- Multiple radial cuts and stretching (not AMR, many research groups)
- AMR on Cartesian grids

CFFC Implementation

- Truly 3D AMR, using unstructured root-block connectivity
- Body-fitted mesh by constraining the points on the boundary spheres

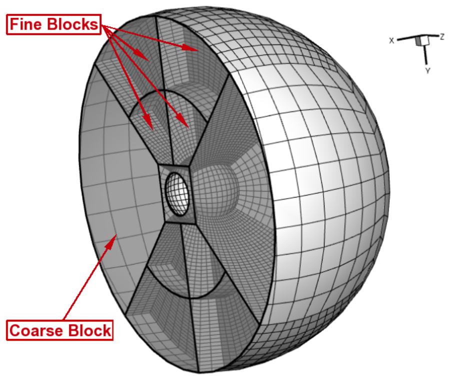

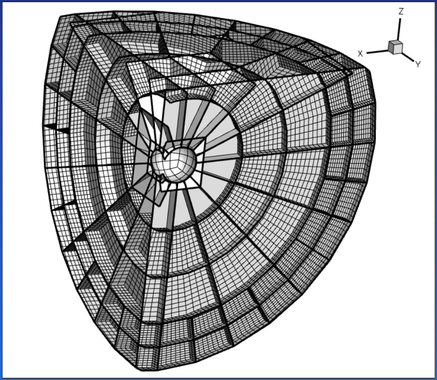

Parallel Adaptive Finite-Volume Framework

Assessment of CFFC Parallel Performance on SciNet GPC (Nehalem processors)

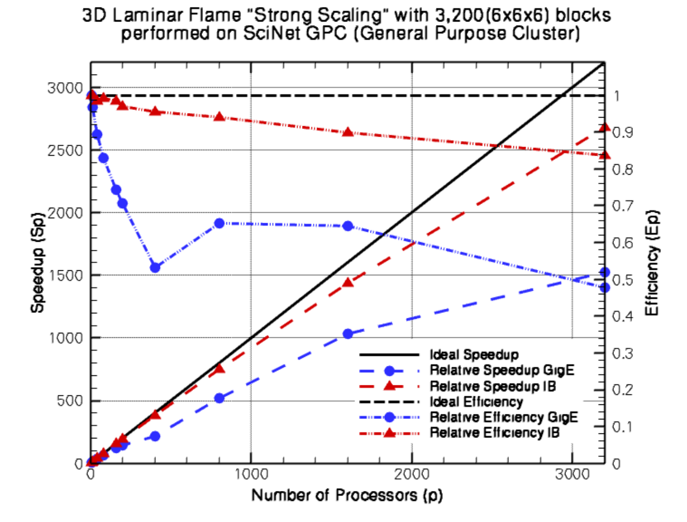

Courtesy of S. Northrup

Numerical Results

Summary of Studied Problems

- Supersonic Outflow
- Transonic Wind on Fixed and AMR Meshes (Radially Symmetric)
- Supersonic Flow Past a Sphere
- Supersonic Rotating Outflow

Numerical Results

Supersonic Inflow Outflow (Hydro, 2nd Order) $R_i = 1$ (Inflow), $R_o = 4$ (Outflow), $GM_* = 0$

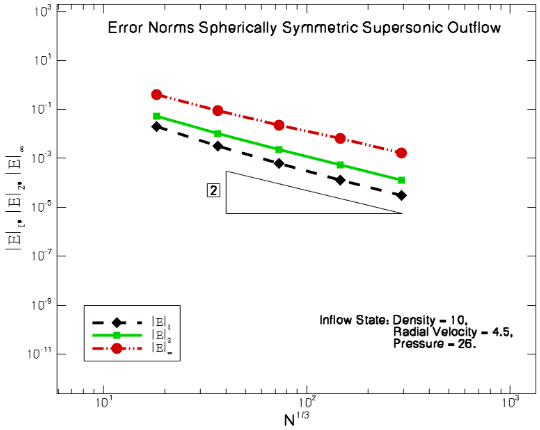

Convergence study based on analytical solution for meshes in the range 6,144 to 25,165,824 total cells

Numerical Results

Transonic Wind (Hydro, 2nd Order) $R_i = 1$, $R_o = 10$, $GM_* = 14$, Inflow: $\rho = 5$, $p = 23$

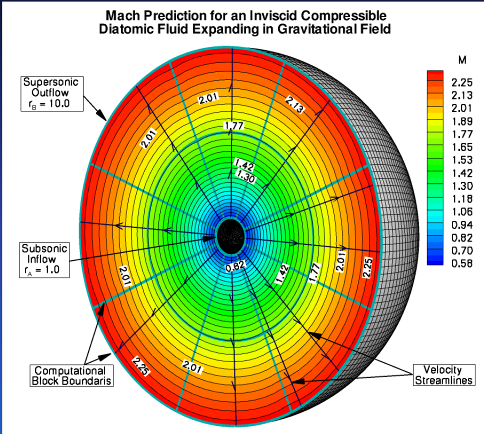

Predicted Mach number distribution obtained on a uniform mesh with 1,228,800 total cells and 128 cells in the radial direction

Numerical Results

Transonic Wind (Hydro, 2nd Order) $R_i = 1$, $R_o = 10$, $GM_* = 14$, Inflow: $\rho = 5$, $p = 23$

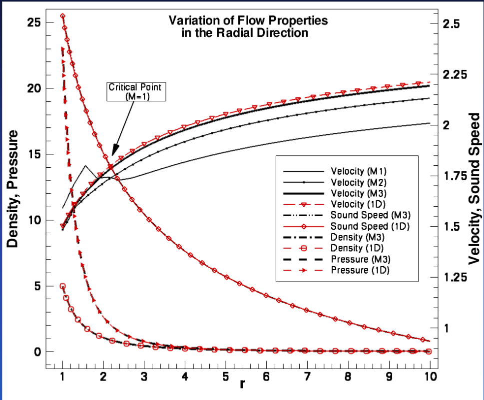

Comparison of flow properties along X-axis for M1 (19,200), M2 (153,600) and M3 (1,228,800) meshes relative to a 1D "exact solution" obtained with Newton Critical Point (NCP) method (De Sterck *et. al.* 2009).

Numerical Results

Transonic Wind on AMR Mesh $R_i = 1$, $R_o = 10$, $GM_* = 14$, Inflow: $\rho = 5$, $p = 23$

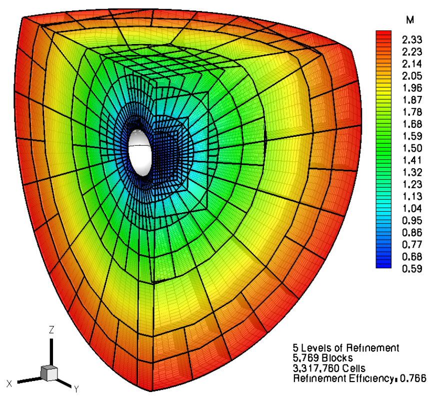

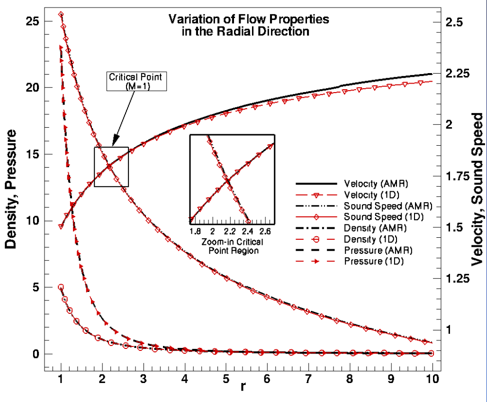

Predicted Mach number distribution obtained on the adapted cubed-sphere mesh. Comparison of flow properties in the X-axis direction.

Numerical Results

Supersonic Flow Past a Sphere (Hydro, 2nd Order) $M_\infty = 2.0,\ R_i = 1,\ R_o = 32,\ GM_* = 0$

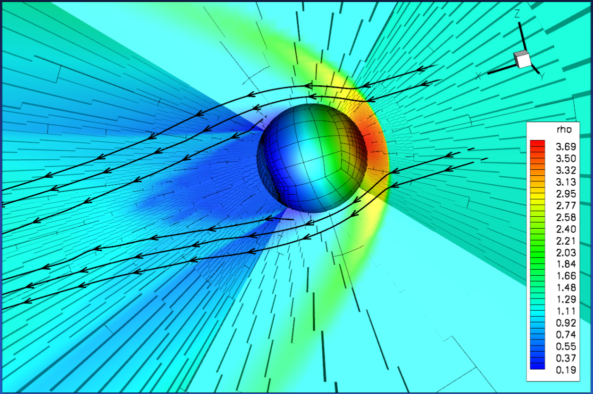

Predicted density distribution on the final refined AMR mesh with 10,835 blocks and 8,321,280 computational cells (7 levels of refinement, $\eta = 0.993$)

Numerical Results

2D Rotating Outflow (MHD, 2nd Order)

$R_i = 1$, $R_o = 6$, $GM_* = 0$, Inflow: $\rho = 1$, $p = 1$, $V_r = 3$, $V_\theta = 1$, $B_r = 1$

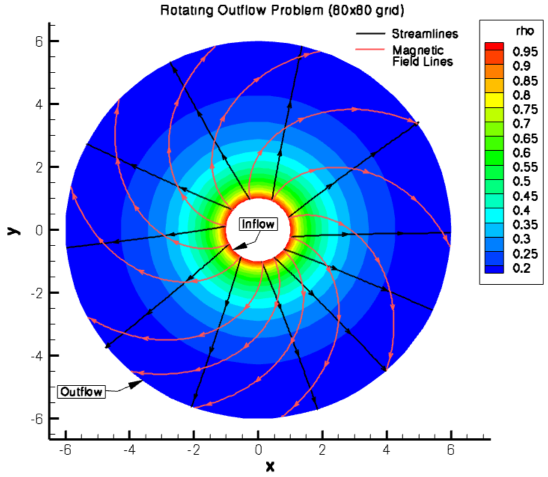

Predicted density field distribution obtained on a mesh with 80×80 cells

Numerical Results

3D Rotating Outflow (MHD, 2nd Order)

$R_i = 1$, $R_o = 6$, $GM_* = 0$, Inflow: $\rho = 1$, $p = 1$, $V_r = 3$, $V_\theta = 1$, $B_r = 1$

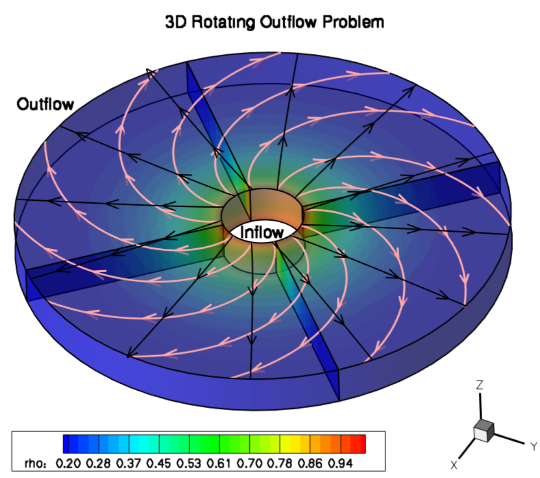

Density distribution obtained on a mesh with 20,160 total cells (70×72 radial)

Concluding Remarks & Ongoing Research

Parallel Block-Based Adaptive Simulation Framework

- Developed for 3D cubed-sphere grids and space-physics flows
- Uses multi-dimensional FVM and gnomonic cubed-sphere grids
- Accuracy assessment based on exact and accurate 1D solutions
- Permits local solution-directed mesh refinement
- Handles and resolves regions of strong discontinuities/shocks

Concluding Remarks & Ongoing Research

Ongoing Research

- High-order on cubed-sphere grid
- $\nabla \cdot \vec{B} = 0$ with high-order
- Improved implicit time integration
- Application of the method to space-physics problems (solar wind, CME)

Acknowledgements

- This work was supported by CSA CGSM Contract No. 9F007-080157/001/ST
- Computations were performed on the GPC supercomputer at the SciNet HPC Consortium